ISSN (Print) : 0974-6846
ISSN (Online) : 0974-5645
Indian Journal of Science and Technology, *Vol 9(30), DOI: 10.17485/ijst/2016/v9i30/97729, August 2016*

Coupling of Adaptive Element Free Galerkin Method with Variational Multiscale Method for Two-Dimensional Sine-Gordon Equation

Siaw-Ching Liew*, Su-Hoe Yeak and Munira Bt. Ismail

Department of Mathematical Sciences, Faculty of Science, Universiti Teknologi Malaysia, UTM Johor Bahru, Johor Darul Ta'azim - 81310, Malaysia; siawching87@yahoo.com

Abstract

In this paper, a coupling of adaptive element free Galerkin method with variational multiscale method is used to solve sine-Gordon equation in two-dimensional for the first time. Meshfree method is used where no mesh regeneration is needed comparing to finite element method. Therefore, this property facilitates the insertion of nodes which is triggered by the adaptive refinement procedure. Additional new nodes will be inserted at the high gradient regions to improve the numerical solutions. The adaptive analysis such as the refinement criteria and refinement strategy will be shown as well as the development of the modified moving least squares approximation. The performance of the proposed method is validated by solving two numerical problems. The first problem is two-dimensional large localized gradient problem with available analytical solution and the second problem is sine-Gordon equation. Numerical results proved that this method can obtain higher accuracy results compared with the conventional element free Galerkin method.

Keywords: Adaptive Analysis, Element Free Galerkin Method, Large Localized Gradient Problem, Sine-Gordon Equation, Variational Multiscale Method

1. Introduction

Over the past few decades, the Finite Element Method (FEM) has been mostly used by researchers in solving engineering and science problems. Researchers have developed adaptive FEM to solve different kind of problems such as limit analysis[1], frictionless contact problems[2] and optical nano structures[3]. However, this mesh-based method has its shortcomings since this numerical method is highly reliance on a mesh. The quality of the mesh is very important for the accuracy of FEM results. An appropriate mesh structures are often difficult to create or modified especially for the adaptive analysis where the meshes must be automatically reconstructed during the computational process. Besides, FEM is also not suitable in dealing with large deformation problems as mesh distortion will occur and this will lead to degradation in accuracy.

Recently, the development of meshfree methods have been gaining attention. The construction of the basis function for meshfree method does not rely on the mesh structure as it only uses nodes scattered in the problem domain to get the approximation. Thus, these meshfree methods are very attractive alternative to FEM since the difficulties of reconstruction of meshes can be avoided. There are many meshfree methods available such as Element Free Galerkin Method (EFGM)[4-6], Smooth Particle Hydrodynamics (SPH) method[7] and Reproducing Kernel Particle Method (RKPM)[5]. A lot of research efforts can be seen in solving problems related

**Author for correspondence*

to adaptive meshfree methods. There are many papers revealed the employment of adaptive refinement procedure for the meshfree methods. For instance, Lee and co-workers[8] have developed adaptive analysis of crack propagation by using element free Galerkin method. Li and Lee[9] have used adaptive meshless method to analyze large deformation and mechanical contact problems. Le and members[10] have employed *h*-adaptive EFGM in the framework of limit analysis of plates. In addition, Zhang and his co-workers have coupled the variational multiscale method[11,12] with element free Galerkin method which is called as variational multiscale EFGM. The concept behind of this technique is the decomposition of the scalar field into two scale parts, namely coarse and the fine scale parts. They have employed this method to solve many numerical problems such as water wave problem[13], stokes problem[14] and incompressible fluid flow[15].

Recently, the soliton-like structure models have attract the attention of researchers. There are many applications involving soliton solutions, for instance, the Josephson junction model possess soliton-like solutions[16] and it is extensively applied in electronics. There is a great number of papers have been published regarding solving sine-Gordon equation with different numerical methods. Dehghan and Shokri[17] have developed a numerical approach to solve two-dimensional sine-Gordon equation which utilizing the radial basis function to get the approximation of the solution. Additionally, Mohebbi and Dehghan[18] have solved the one-dimensional nonlinear sine-Gordon equation with using a compact finite difference scheme to discretize the spatial derivative and diagonally implicit Runge-Kutta-Nyström method in dealing with time integration.

The objective of this paper is to couple the adaptive element free Galerkin method with the variational multiscale method to solve sine-Gordon equation in two dimension. The layout of the paper is arranged as: Section 2 presents the modified moving least square approximation and the development of shape function. Section 3 introduces the adaptive analysis techniques such as the refinement criteria and node insertion strategy. In section 4, two numerical problems will be solved by using the proposed method. Firstly, a two-dimensional large localized gradient problem with available analytical solution is solved in order to prove the effectiveness of the proposed method. After that, this method will also be employed to get the solutions of two-dimensional sine-Gordon equation. In this section, the description of variational multiscale element free Galerkin method as well as the numerical procedures will be shown. Lastly, the conclusions will be presented in Section 5.

2. Modified Moving Least Squares Approximation

The derivation of modified moving least squares approximation will be illustrated in this section. In EFGM shape function, the function $u(\mathbf{x})$ is approximated as $u^h(\mathbf{x})$ by using moving least square (MLS) approximation. So, the MLS approximation can be given by

$$u^h(\mathbf{x}) = \sum_{i=1}^{m} p_i(\mathbf{x}) a_i(\mathbf{x}) = \mathbf{p}^{\mathrm{T}}(\mathbf{x})\mathbf{a}(\mathbf{x}) \tag{1}$$

where $\mathbf{p}(\mathbf{x})$ is the basis functions, m indicates the number of the basis functions and $\mathbf{a}(\mathbf{x})$ is an unknown vector of the coefficients. The linear basis in two dimension is given by

$$\mathbf{p}^{\mathrm{T}}(\mathbf{x}) = (1, x, y) \tag{2}$$

In the present work, the adaptive element free Galerkin method is coupled with the variational multiscale method. Therefore, the variational multiscale concept has been incorporated into the local approximation $u^h(\mathbf{x})$. The approximation $u^h(\mathbf{x})$ is assumed as the summation of the coarse scale part and fine scale part as follows:

$$u^h(\mathbf{x}) = \bar{u}^h(\mathbf{x}) + \hat{u}^h(\mathbf{x}) = \mathbf{p}^{\mathrm{T}}(\mathbf{x})\bar{\boldsymbol{a}}(\mathbf{x}) + \mathbf{p}^{\mathrm{T}}(\mathbf{x})\hat{\boldsymbol{a}}(\mathbf{x}) \tag{3}$$

where "–"represents coarse scale part while "^" represents fine scale part. The two unknown coefficients $\bar{\boldsymbol{a}}(\mathbf{x})$ and $\hat{\boldsymbol{a}}(\mathbf{x})$ are determined separately according to

the fine scale part and coarse scale part. The unknown coefficient from coarse scale part, $\bar{\boldsymbol{a}}(\mathbf{x})$ can be obtained by applying weighted least-square fitting to the local approximation given by

$$\bar{J} = \sum_{I^*=1}^{N} w(\mathbf{x}-\mathbf{x}_{I^*})\left[\bar{u}^h(\mathbf{x}) - \bar{u}_{I^*}\right]^2 = \sum_{I^*=1}^{N} w(\mathbf{x}-\mathbf{x}_{I^*})\left[\mathbf{p}^{\mathrm{T}}(\mathbf{x}_{I^*})\bar{\mathbf{a}}(\mathbf{x}) - \bar{u}_{I^*}\right]^2, \tag{4}$$

where $w(\mathbf{x}-\mathbf{x}_{I^*})$ is defined as the weight function, $\bar{u}_{I^*}$ represents the nodal value for both original nodes and new nodes since N is defined as follows

$$\mathrm{N} = \mathrm{I} + \mathrm{J} \tag{5}$$

where I indicates the number of original nodes and J indicates the number of new nodes. Next, the fine scale unknown coefficient $\hat{\boldsymbol{a}}(\mathbf{x})$ can be obtained by introducing a special enrichment function in minimizing the following weighted, discrete error norm as

$$\hat{J} = \sum_{I^*=1}^{N} w(\mathbf{x}-\mathbf{x}_{I^*})(\mathbf{x}-\mathbf{x}_{I^*})^2(\mathbf{y}-\mathbf{y}_{I^*})^2\left[\mathbf{p}^{\mathrm{T}}(\mathbf{x}_{I^*})\hat{\mathbf{a}}(\mathbf{x}) - \hat{u}_{I^*}\delta_{I^*\mathrm{J}}\right]^2 \tag{6}$$

A Kronecker delta $\ddot{a}_{I^*\mathrm{J}}$ is introduced in (6) for the purpose to enforce the nodal values of u are only involve fine nodes. Consequently, the term $\hat{u}_{I^*}\ddot{a}_{I^*\mathrm{J}}$ is similar to $\hat{u}_{\mathrm{J}}$ as these nodal values are only for fine nodes. Thereafter, the unknown coefficient $\bar{\boldsymbol{a}}(\mathbf{x})$ is obtained by minimum of $\bar{J}$ in (4) with respect to $\bar{\boldsymbol{a}}(\mathbf{x})$ leads to

$$\mathbf{A}(\mathbf{x})\bar{\boldsymbol{a}}(\mathbf{x}) = \mathbf{B}(\mathbf{x})\bar{\mathbf{u}} \tag{7}$$

After rearranged, $\bar{\boldsymbol{a}}(\mathbf{x})$ is written as

$$\bar{\boldsymbol{a}}(\mathbf{x}) = \mathbf{A}^{-1}(\mathbf{x})\mathbf{B}(\mathbf{x})\bar{\mathbf{u}}. \tag{8}$$

The matrix $\mathbf{A}(\mathbf{x})$ and $\mathbf{B}(\mathbf{x})$ for the coarse scale part are given as

$$\mathbf{A}(\mathbf{x}) = \sum_{I^*=1}^{N} w(\mathbf{x}-\mathbf{x}_{I^*})\mathbf{p}(\mathbf{x}_{I^*})\mathbf{p}^{\mathrm{T}}(\mathbf{x}_{I^*}), \tag{9}$$

$$\mathbf{B}(\mathbf{x}) = \left[w(\mathbf{x}-\mathbf{x}_1)\mathrm{p}(\mathbf{x}_1), w(\mathbf{x}-\mathbf{x}_2)\mathrm{p}(\mathbf{x}_2), \cdots, w(\mathbf{x}-\mathbf{x}_{\mathrm{N}})\mathrm{p}(\mathbf{x}_{\mathrm{N}})\right] \tag{10}$$

Next, we need to get the fine scale unknown coefficients $\hat{\boldsymbol{a}}(\mathbf{x})$ as this is the significant part of this paper. Follow the similar way as the derivation for the coarse scale part, the stationarity of $\hat{J}$ in (6) with respect to $\hat{\boldsymbol{a}}(\mathbf{x})$ gives

$$\mathbf{A}(\mathbf{x})\hat{\mathbf{a}}(\mathbf{x}) = \mathbf{B}(\mathbf{x})\hat{\mathbf{u}}, \tag{11}$$

Similarly

$$\hat{\mathbf{a}}(\mathbf{x}) = \mathbf{A}^{-1}(\mathbf{x})\mathbf{B}(\mathbf{x})\hat{\mathbf{u}}. \tag{12}$$

Thus, the new matrix of $\mathbf{A}(\mathbf{x})$ and $\mathbf{B}(\mathbf{x})$ are developed for the fine scale part with the new added enrichment function given as follows:

$$\mathbf{A}(\mathbf{x}) = \sum_{I^*=1}^{N} w(\mathbf{x}-\mathbf{x}_{I^*})(\mathbf{x}-\mathbf{x}_{I^*})^2(\mathbf{y}-\mathbf{y}_{I^*})^2\mathbf{p}(\mathbf{x}_{I^*})\mathbf{p}^{\mathrm{T}}(\mathbf{x}_{I^*}), \tag{13}$$

$$\mathbf{B}_{\mathrm{J}}(\mathbf{x}) = w(\mathbf{x}-\mathbf{x}_{\mathrm{J}})(\mathbf{x}-\mathbf{x}_{\mathrm{J}})^2(\mathbf{y}-\mathbf{y}_{\mathrm{J}})^2\mathbf{p}(\mathbf{x}_{\mathrm{J}}). \tag{14}$$

The approximation $u^h(\mathbf{x})$ can be obtained by substi-

tuting $\bar{\boldsymbol{a}}(\boldsymbol{x})$ and $\hat{\boldsymbol{a}}(\boldsymbol{x})$ obtained from (8) and (12) into (3),

$$u^h(\mathbf{x}) = \bar{\mathbf{o}}^{\mathrm{T}}(\mathbf{x})\bar{\mathbf{u}} + \hat{\mathbf{o}}^{\mathrm{T}}(\mathbf{x})\hat{\mathbf{u}}\,. \tag{15}$$

Different notation are used to distinguish the coarse scale shape function, $\bar{\mathbf{o}}$ and fine scale shape function, $\hat{\mathbf{o}}$. The approximation $u^h(\mathbf{x})$ can be written as

$$u^h(\mathbf{x}) = \sum_{\mathrm{I}^*=1}^{\mathrm{N}} \bar{o}_{\mathrm{I}^*}(\mathbf{x})\bar{u}_{\mathrm{I}^*} + \sum_{\mathrm{J}=1}^{\mathrm{M}} \hat{o}_{\mathrm{J}}(\mathbf{x})\hat{u}_{\mathrm{J}}\,, \tag{16}$$

where M represents the number of new nodes. Since the moving least squares shape function does not verify the Kronecker delta property. So, penalty method[19] is adopted to impose the essential boundary conditions in the present work.

3. Adaptive Analysis

3.1 Refinement Criteria Based on Gradient of Nodes

In adaptive analysis, the refinement criteria is very important to identify the areas where the refinement technique should be employed. In the previous literature, additional nodes will be created at the high stress or large error locations. In order to estimate the error, there are many techniques available in the literature. For this work, the refinement criteria is based on the gradient of each node. Additional nodes will be introduced at the high gradient areas or critical areas to improve the numerical solutions effectively. The technique used to get the gradient of each node is provided as

$$G_m = \sqrt{\left[\sum_{\mathrm{I}^*=1}^{\mathrm{N}} \ddot{\mathrm{o}}_{\mathrm{I}^*,x}(x_m, y_m)u_{\mathrm{I}^*}\right]^2 + \left[\sum_{\mathrm{I}^*=1}^{\mathrm{N}} \ddot{\mathrm{o}}_{\mathrm{I}^*,y}(x_m, y_m)u_{\mathrm{I}^*}\right]^2} \tag{17}$$

where m and I^* are the index of nodes. The nodal refinement strategy is controlled by the following

$$G_m \geq q \quad \text{refine} \tag{18}$$

where q is the threshold value. Once the gradient of node m is exceeding the threshold value, more new nodes will be automatically inserted to its surrounding. A higher value of q was used so that the refinement technique will only adopted at high gradient regions. Besides, smaller support size is used for the new added nodes.

3.2 Refinement Strategy

According to equation (18), additional new nodes will be generated at the corresponding area if the gradient of a node exceeds the threshold value,. To illustrate the refinement strategy clearly, the refinement scheme is shown in figure 1. Based on the figure, eight new nodes will be automatically created once the high gradient node is defined.

The coordinates of eight new nodes are given as:

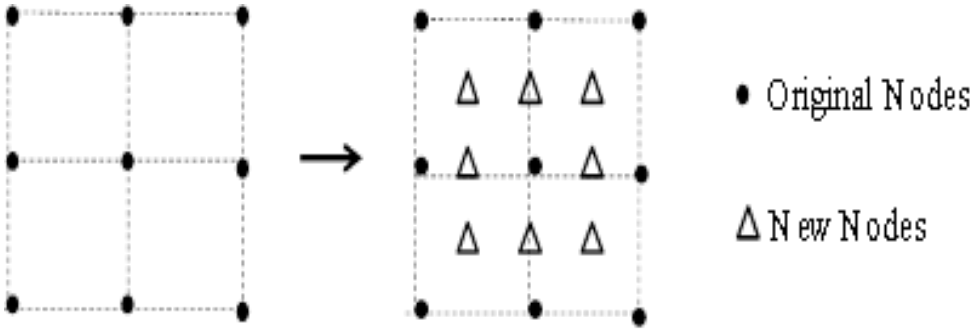

Figure 1. Node refinement technique.

$$\left(x_I-\frac{d_{\mathrm{IM}}}{2},y_I+\frac{d_{\mathrm{IM}}}{2}\right),\quad \left(x_I,y_I+\frac{d_{\mathrm{IM}}}{2}\right),\quad \left(x_I+\frac{d_{\mathrm{IM}}}{2},y_I+\frac{d_{\mathrm{IM}}}{2}\right),\quad \left(x_I-\frac{d_{\mathrm{IM}}}{2},y_I\right),\quad \left(x_I+\frac{d_{\mathrm{IM}}}{2},y_I\right),$$
$$\left(x_I-\frac{d_{\mathrm{IM}}}{2},y_I-\frac{d_{\mathrm{IM}}}{2}\right),\ \left(x_I,y_I-\frac{d_{\mathrm{IM}}}{2}\right),\ \left(x_I+\frac{d_{\mathrm{IM}}}{2},y_I-\frac{d_{\mathrm{IM}}}{2}\right)$$

where d_{M} is the distance between neighboring nodes.

4. Variational Multiscale Element Free Galerkin Method

4.1 High Gradient Problem

A two-dimensional localized large gradient problem is solved by using the proposed coupling method. This problem is defined over the square domain $\Omega=[0,1]\times[0,1]$ defined as

$$\frac{\partial u}{\partial t}=\frac{\partial^2 u}{\partial x^2}+\frac{\partial^2 u}{\partial y^2}+f(x,y) \tag{19}$$

where

$$f(x,y)=-e^{-\gamma^2(x-0.5)^2}\beta e^{-\beta t}+2\gamma^2 e^{-\gamma^2(x-0.5)^2}e^{-\beta t}-4\gamma^4(x-0.5)^2 e^{-\gamma^2(x-0.5)^2}e^{-\beta t}. \tag{20}$$

Here, the following conditions are given as

$$u(x,y,0)=x+e^{-\gamma^2(x-0.5)^2}+1, \tag{21}$$

$$u(0,y,t)=g_0(y,t)\quad u(1,y,t)=g_1(y,t) \tag{22}$$

$$u(x,0,t)=g_2(x,t)\quad u(x,1,t)=g_3(x,t) \tag{23}$$

The analytical solution for equation (19) is defined as

$$u(x,y,t)=x+e^{-\gamma^2(x-0.5)^2}e^{-\beta t}+1. \tag{24}$$

The weak form is obtained by multiplying both sides of equation (19) by an admissible weighting function. Taking backward Euler time discretization and adopting penalty method to enforce essential boundary conditions. Next, integrating it over the domain to get

$$\left(w,\frac{u^{n+1}}{\Delta t}\right)+\left(\nabla w,\nabla u^{n+1}\right)+\alpha\int_{\Gamma_u} wu^{n+1}d\Gamma=\left(w,\frac{u^n}{\Delta t}\right)+\int_{\Gamma} w\nabla u\cdot nd\Gamma+(w,f)+\alpha\int_{\Gamma_u} wu_E d\Gamma, \tag{25}$$

where w is the weighting function, α is the penalty parameter, u_E is the displacement on essential boundary and $(\cdot,\cdot)=\int_\Omega(\cdot)\,d\Omega$. In variational multiscale method, the velocity u and weighting function w are assumed can be decomposed into two scales, in which coarse scale and fine scale described as

$$u=\overline{u}+\hat{u}\,, \tag{26}$$

$$w=\overline{w}+\hat{w}\,. \tag{27}$$

After that, the trial solutions (26) and (27) are substituted into (25) to get

$$\begin{aligned}&\left(\overline{w}+\hat{w},\frac{\overline{u}^{n+1}+\hat{u}^{n+1}}{\Delta t}\right)+\left(\nabla\left(\overline{w}+\hat{w}\right),\nabla\left(\overline{u}^{n+1}+\hat{u}^{n+1}\right)\right)+\alpha\int_{\Gamma_u}\left(\overline{w}+\hat{w}\right)\left(\overline{u}^{n+1}+\hat{u}^{n+1}\right)d\Gamma\\&=\left(\overline{w}+\hat{w},\frac{u^n}{\Delta t}\right)+\int_\Gamma\left(\overline{w}+\hat{w}\right)\nabla u\cdot n\,d\Gamma+\left(\overline{w}+\hat{w},f\right)+\alpha\int_{\Gamma_u}\left(\overline{w}+\hat{w}\right)u_E\,d\Gamma.\end{aligned} \tag{28}$$

Next, equation (28) can be split into coarse scale and fine scale parts as follows:

$$\begin{aligned}&\overline{W}:\left(\overline{w},\frac{\overline{u}^{n+1}+\hat{u}^{n+1}}{\Delta t}\right)+\left(\nabla\overline{w},\nabla\left(\overline{u}^{n+1}+\hat{u}^{n+1}\right)\right)+\alpha\int_{\Gamma_u}\overline{w}\left(\overline{u}^{n+1}+\hat{u}^{n+1}\right)d\Gamma\\&=\left(\overline{w},\frac{u^n}{\Delta t}\right)+\int_\Gamma\overline{w}\nabla u\cdot n\,d\Gamma+\left(\overline{w},f\right)+\alpha\int_{\Gamma_u}\overline{w}u_E\,d\Gamma\end{aligned} \tag{29}$$

$$\begin{aligned}&\hat{W}:\left(\hat{w},\frac{\overline{u}^{n+1}+\hat{u}^{n+1}}{\Delta t}\right)+\left(\nabla\hat{w},\nabla\left(\overline{u}^{n+1}+\hat{u}^{n+1}\right)\right)+\alpha\int_{\Gamma_u}\hat{w}\left(\overline{u}^{n+1}+\hat{u}^{n+1}\right)d\Gamma\\&=\left(\hat{w},\frac{u^n}{\Delta t}\right)+\int_\Gamma\hat{w}\nabla u\cdot n\,d\Gamma+\left(\hat{w},f\right)+\alpha\int_{\Gamma_u}\hat{w}u_E\,d\Gamma\end{aligned} \tag{30}$$

Rearranging equations (29) and (30) becomes

$$\begin{aligned}&\overline{W}:\left(\overline{w},\frac{\overline{u}^{n+1}}{\Delta t}\right)+\left(\nabla\overline{w},\nabla\overline{u}^{n+1}\right)+\alpha\int_{\Gamma_u}\overline{w}\overline{u}^{n+1}d\Gamma=\left(\overline{w},\frac{u^n}{\Delta t}\right)+\int_\Gamma\overline{w}\nabla u\cdot n\,d\Gamma+\left(\overline{w},f\right)\\&\quad+\alpha\int_{\Gamma_u}\overline{w}u_E\,d\Gamma-\left(\overline{w},\frac{\hat{u}^{n+1}}{\Delta t}\right)-\left(\nabla\overline{w},\nabla\hat{u}^{n+1}\right)-\alpha\int_{\Gamma_u}\overline{w}\hat{u}^{n+1}d\Gamma\end{aligned} \tag{31}$$

$$\hat{W}:\left(\hat{w},\frac{\hat{u}^{n+1}}{\Delta t}\right)+\left(\nabla\hat{w},\nabla\hat{u}^{n+1}\right)+\alpha\int_{\Gamma_u}\hat{w}\hat{u}^{n+1}d\Gamma=\left(\hat{w},\frac{u^{n}}{\Delta t}\right)+\int_{\Gamma}\hat{w}\nabla u\cdot\mathbf{d}\ \Gamma+\left(\hat{w},f\right)$$
$$+\alpha\int_{\Gamma_u}\hat{w}u_E d\Gamma-\left(\hat{w},\frac{\overline{u}^{n+1}}{\Delta t}\right)-\left(\nabla\hat{w},\nabla\overline{u}^{n+1}\right)-\alpha\int_{\Gamma_u}\hat{w}\overline{u}^{n+1}d\Gamma. \quad (32)$$

In order to get the numerical results, equations (31) and (32) must be solved iteratively with the following solution procedures:

(1) $\overline{u}^{n+1,0}=u^{n}$;

(2) The fine scale problem is solved by replacing the coarse variable $\overline{u}^{n+1}$ in the right-hand side with $\overline{u}^{n+1,i}$ to get $\hat{u}^{n+1,i+1}$;

$$\hat{W}:\left[K_1^{n+1,\,i+1}\right]\left\{\hat{u}^{n+1,\,i+1}\right\}=\left(\hat{w},\frac{u^{n}}{\Delta t}\right)+\int_{\Gamma}\hat{w}\nabla u\cdot\mathbf{d}\ \Gamma+\left(\hat{w},f\right)+\alpha\int_{\Gamma_u}\hat{w}u_E d\Gamma-\left\{F_1\left(\overline{u}^{n+1,i}\right)\right\}.$$

(3) The coarse scale problem is solved by substituting the fine scale results into the right hand side of the coarse scale problem

$$\overline{W}:\left[K_2^{n+1,\,i+1}\right]\left\{\overline{u}^{n+1,\,i+1}\right\}=\left(\overline{w},\frac{u^{n}}{\Delta t}\right)+\int_{\Gamma}\overline{w}\nabla u\cdot\mathbf{d}\ \Gamma+\left(\overline{w},f\right)+\alpha\int_{\Gamma_u}\overline{w}u_E d\Gamma-\left\{F_2\left(\hat{u}^{n+1,\,i+1}\right)\right\}$$

(4) Employ equation (16) to get $u_{\text{real}}^{n+1,i}$ and $u_{\text{real}}^{n+1,i+1}$, then compute

error=max$\left|u_{\text{real}}^{n+1,i+1}-u_{\text{real}}^{n+1,i}\right|$;

(5) If error <10^{-5}, let $u^{n+1,i+1}\rightarrow u^{n}, n+1\rightarrow n$ and

go to step (1), or else continue with step (2).

The numerical results are obtained with the node distribution 14×14. The linear basis will be used in the entire work with scalar parameter 2.5. The parameters $\gamma=20$ and $\beta=0.1$ are adopted and the penalty parameter $\alpha=5000$ is employed. Figure 2 illustrates the numerical results at $t=0.2$ on node distribution 14×14. While figure 3 shows the refined nodal arrangement of figure 2. It can be observed that the additional nodes are inserted at the large gradient area in order to improve the solution accuracy. The relative errors for the domain surface are shown in figure 4. Based on the figure, the relative errors for the adaptive EFGM are smaller than the EFGM.

Figure 5 shows the average relative error of the proposed coupling method and the standard EFGM on 14×14 nodes. According to the figure, it can be seen that the average relative errors for the adaptive EFGM are smaller than the standard EFGM. This adaptive EFGM with the added special enrichment function for the fine scale part is able to improve the solution accuracy. Thus, it can be conclude that this proposed method is accurate and effective.

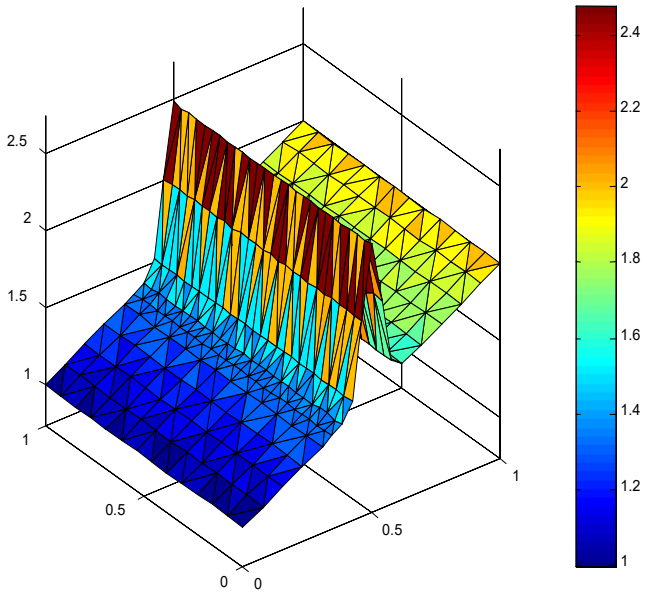

Figure 2. The numerical results at t=0.2 with .

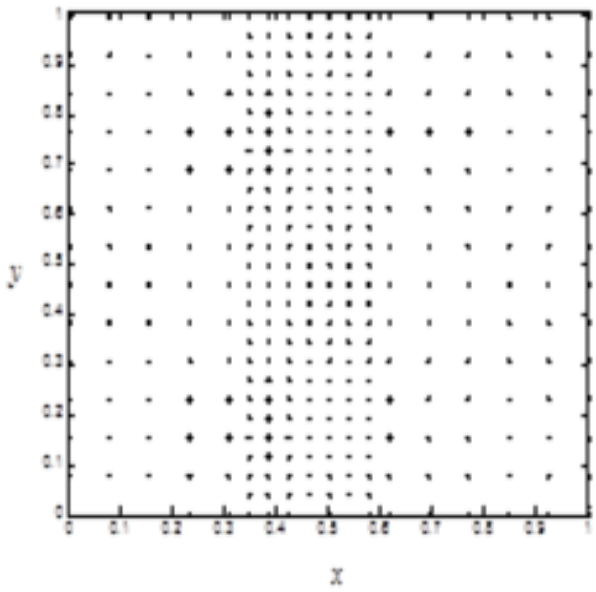

Figure 3. Refined nodal arrangement of figure 2 at t = 0.2.

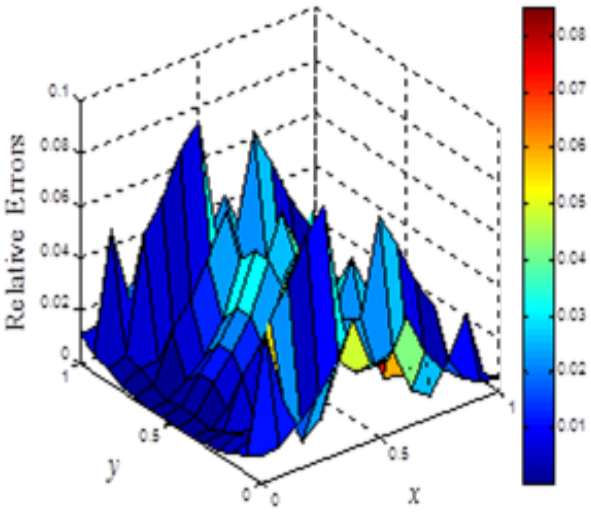

(a)

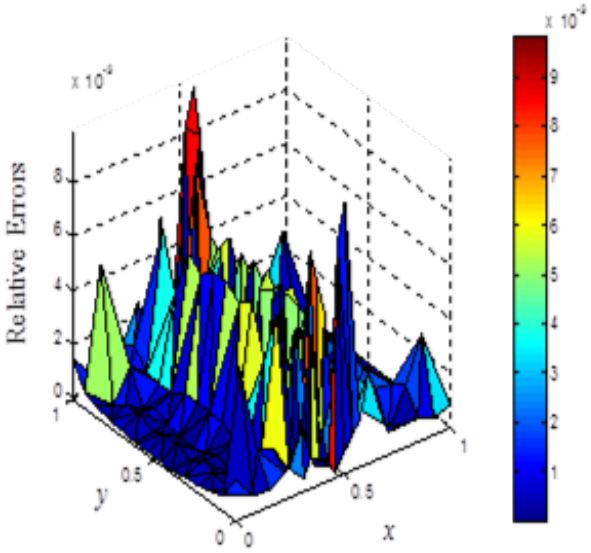

(b)

Figure 4. The relative errors at node (a) EFGM (b) Adaptive EFGM.

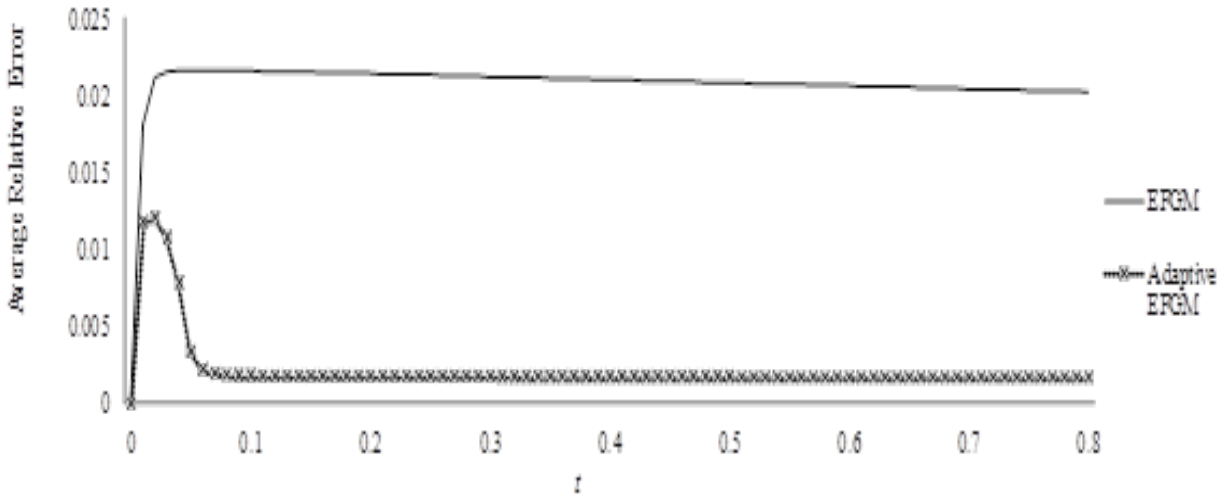

Figure 5. The average relative error of adaptive EFGM and EFGM on 14×14 nodes.

4.2 Two-Dimensional Sine-Gordon Equation

In this section, the coupling method proposed in this work will be adopted to solve two-dimensional sine-Gordon equation for the first time. Consider the sine-Gordon equation in two dimension is described as

$$\frac{\partial^2 u}{\partial t^2}+\beta\frac{\partial u}{\partial t}=\frac{\partial^2 u}{\partial x^2}+\frac{\partial^2 u}{\partial y^2}-\phi(x,y)\sin(u) \qquad (33)$$
$$(x,y)\in\Omega,\ t>0$$

The initial conditions are defined as

$$u(x,y,0)=4\tan^{-1}\left(\exp\left(x+1-2\sec h(y+7)-2\sec h(y-7)\right)\right),\quad -7\le x,y\le 7, \qquad (34)$$

$$\frac{\partial u}{\partial t}(x,y,0)=0,\quad -7\le x,y\le 7. \qquad (35)$$

While the boundary conditions are provided as

$$\frac{\partial u}{\partial x}=0 \ \text{ for } x=-7 \ \text{ and } \ x=7, \qquad (36)$$

$$\frac{\partial u}{\partial y}=0 \ \text{ for } y=-7 \ \text{ and } \ y=7. \qquad (37)$$

The weak form is obtained by multiplying equation (33) with the weight function to get

$$\int_\Omega w\frac{\partial^2 u}{\partial t^2}d\Omega+\int_\Omega w\frac{\beta\partial u}{\partial t}d\Omega=\int_\Gamma w\nabla u\cdot nd\Gamma-\int_\Omega \nabla w\cdot\nabla u d\Omega-\int_\Omega w\phi(x,y)\sin(u)d\Omega \qquad (38)$$

Next, applying central difference method for time derivatives to get

$$\int_{\Omega} w\frac{u^{n+1}}{\Delta t^2}d\Omega+\int_{\Omega} w\frac{\beta u^{n+1}}{2\Delta t}d\Omega=2\int_{\Omega} w\frac{u^{n}}{\Delta t^2}d\Omega-\int_{\Omega} w\frac{u^{n-1}}{\Delta t^2}d\Omega+\int_{\Omega} w\frac{\beta u^{n-1}}{2\Delta t}d\Omega$$
$$-\int_{\Omega}\nabla w\cdot\nabla d\ \ \Omega-\int_{\Omega} w\phi(x,y)\sin(u)d\Omega \tag{39}$$

where n denotes time level. Follow the similar way as in section 4.1, the coarse scale part and the fine scale part are indicated as

$$\overline{W}:\left(\overline{w},\frac{\overline{u}^{n+1}}{\Delta t^2}\right)+\left(\overline{w},\frac{\beta\overline{u}^{n+1}}{2\Delta t}\right)=\left(\overline{w},\frac{2u^{n}}{\Delta t^2}\right)-\left(\overline{w},\frac{u^{n-1}}{\Delta t^2}\right)+\left(\overline{w},\frac{\beta u^{n-1}}{2\Delta t}\right)-\left(\nabla\overline{w},\nabla u\right)$$
$$-\left(\overline{w},\phi(x,y)\sin(u)\right)-\left(\overline{w},\frac{\hat{u}^{n+1}}{\Delta t^2}\right)-\left(\overline{w},\frac{\beta\hat{u}^{n+1}}{2\Delta t}\right) \tag{40}$$

$$\hat{W}:\left(\hat{w},\frac{\hat{u}^{n+1}}{\Delta t^2}\right)+\left(\hat{w},\frac{\beta\hat{u}^{n+1}}{2\Delta t}\right)=\left(\hat{w},\frac{2u^{n}}{\Delta t^2}\right)-\left(\hat{w},\frac{u^{n-1}}{\Delta t^2}\right)+\left(\hat{w},\frac{\beta u^{n-1}}{2\Delta t}\right)-\left(\nabla\hat{w},\nabla u\right)$$
$$-\left(\hat{w},\phi(x,y)\sin(u)\right)-\left(\hat{w},\frac{\overline{u}^{n+1}}{\Delta t^2}\right)-\left(\hat{w},\frac{\beta\overline{u}^{n+1}}{2\Delta t}\right) \tag{41}$$

This problem is solved numerically in the domain $-7\le x,\ y\le 7$ with the parameters $\beta=0.05,\phi(x,y)=1,$ $\Delta t=0.04$, $\alpha=5000$ and grid size 15×15 are employed in the region. The numerical procedures used are similar in section 4.1 in order to get the results. The numerical results are plotted in terms of $\sin(u/2)$ at $t=2.$

Figure 6 illustrates the numerical results of perturbation of a single soliton for $\beta=0.05,\phi(x,y)=1,\Delta t=0.04$ at t =2 on 15×15 nodes. This graph is in a good agreement with Dehghan and Shokri (2008) work. Besides, figure 7 shows the refined nodal arrangement of figure 6. Based on the figure, the additional nodes are concentrated at the steep gradient area to refine the solution. Thus, the refinement criteria based on the gradient of node is suitable to estimate the location of the refined nodes in order to improve the accuracy.

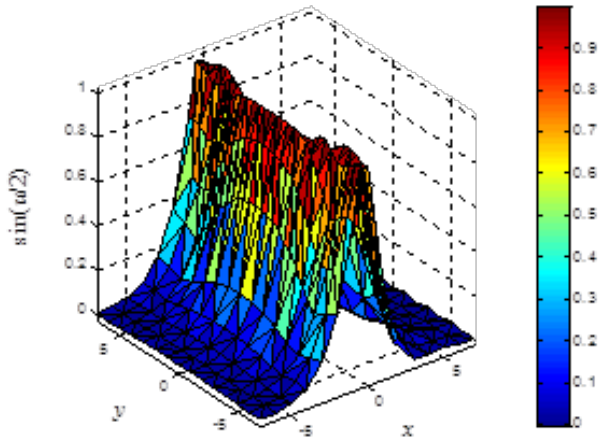

Figure 6. Numerical solutions at t =2 with on nodes.

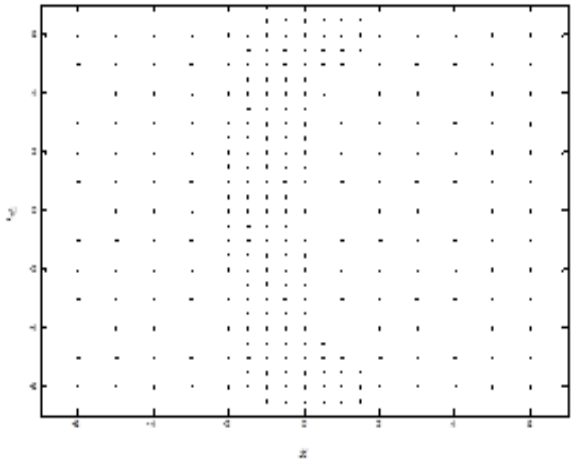

Figure 7. Refined nodal arrangement of figure 6 at .

5. Conclusions

A coupling of adaptive element free Galerkin method with variational multiscale method is employed in two-dimensional sine-Gordon problem in this paper. A special enrichment function is adopted for the development of the fine scale part shape function. Here, the refinement criteria is based on the gradient for each node. Additional new nodes will be inserted once the gradient of a node is exceeding the threshold value. According to the results obtained, the refined nodes are concentrated at the appropriate high gradient regions to improve the numerical results. Moreover, the numerical results show higher accuracy than the standard EFGM as the relative errors and average relative errors for the proposed method are smaller than the standard EFGM. For the sine-Gordon problem, the numerical solutions are agree well with the extant published results and the new nodes are located at the steep gradient regions. Therefore, this coupling method is good, accurate and suitable to solve more high gradient problems to get higher accuracy results.

6. Acknowledgements

The financial support from MyBrain15 (MyPhD), Kementerian Pengajian Tinggi Malaysia and Fundamental Research Grant Scheme (R.J130000.7826.4F623), Universiti Teknologi Malaysia are fully acknowledged.

6. References

1. Lavinia B, Nestor Z, Cyntia C, Raul F. An adaptive approach to limit analysis. International Journal of Solids and Structures. 2001; 38:1707–20.
2. Gustavo CB, Ricardo D, Eduardo AF, Raul AF, Claudio P. An adaptive finite element approach for frictionless contact problems. International Journal for Numerical Methods in Engineering. 2001; 50:395–418.
3. Jan P, Sven B, Lin Z, Frank S. Adaptive finite element method for simulation of optical nano structures. Basic Solid State Physics. 2007; 244(10):3419–34.
4. Belytschko T, Lu YY, Gu L. Element-free Galerkin methods. International Journal for Numerical Methods in Engineering. 1994; 37:229–56.
5. Belytschko T, Krongauz Y, Organ D, Fleming M, Krysl P. Meshless method: An overview and recent developments. Computer Methods in Applied Mechanics and Engineering. 1996; 139(1-4):3–47.
6. Liu GR, Gu YT. An introduction to Meshfree Methods and Their Programming. Berlin and New York: Springer, 2005.
7. Gingold RA, Monaghan JJ. Smoothed particle hydrodynamics: theory and application to non spherical stars. Monthly Notices R Astron Soc.1977; 181:375–89.

8. Lee GH, Chung HJ, Choi CK. Adaptive crack propagation analysis with the element free Galerkin method. International Journal for Numerical Methods in Engineering. 2003; 56:331¬–50.
9. Li Q, Lee KM. An adaptive Meshless Method for Analyzing Large Mechanical Deformation and Contacts. Journal of Applied Mechanics. 2008; 75(4):041014 1–9.
10. Le CV, Askes H, Gilbert M. Adaptive Element-Free Galerkin method applied to the limit analysis of plates. Computer Methods in Applied Mechanics and Engineering. 2010; 199(37-40):2487–96.
11. Hughes TJR. Multiscale phenomena: Green's function, the Dirichlet-to-Neumann formulation, subgrid scale models, bubbles and the origins of stabilized methods. Comput Methods Appl Mech Eng.1995; 127:387–401.
12. Hughes TJR, Feijoo GR, Luca M, Baptiste QJ. The variational multiscale method-a paradigm for computational mechanics. Comput Mehtods Appl Mech Eng.1998; 166:3–24.
13. Zhang L, Ouyang J, Jiang T, Ruan CL. Variational multiscale element free Galerkin method for the water wave problems. Journal of Computational Physics. 2011; 230:5045–60.
14. Zhang L, Ouyang J, Zhang XH, Zhang WB. On a multiscale element free Galerkin method for the Stokes problem. Applied Mathematics and Computation. 2008; 203:745–53.
15. Zhang L, Ouyang J, Zhang XH. On a two level element-free Galerkin method for incompressible fluid flow. Applied Numerical Mathematics. 2009; 59:1894–904.
16. Bratsos AG. The solution of the two-dimensional sine-Gordon equation using the method of lines. J Comput Appl Math. 2007; 206:251–77.
17. Dehghan M, Shokri A. A numerical method for solution of the two-dimensional sine Gordon equation using the radial basis functions. Mathematics and Computers in Simulation. 2008; 79:700–15.
18. Mohebbi A, Dehghan M. High-order solution of one-dimensional sine-Gordon equation using compact finite difference and DIRKN methods. Mathematical and Computer Modelling. 2010; 51:537–49.
19. Zhu T, Atluri SN. A modified collocation method and a penalty formulation for enforcing the essential boundary conditions in the element free Galerkin method. Computational Mechanics. 1998; 21(3):211–22.